CrystEngComm

ROYAL SOCIETY OF CHEMISTRY

www.rsc.org/crystengcomm

Defects reduction in semipolar $\{10\bar{1}\bar{3}\}$ GaN grown on m-sapphire via two-step nanoepitaxial lateral overgrowth

Jiankun Yang, Tongbo Wei*, Ziqiang Huo, Yonghui Zhang, Qiang Hu, Xuecheng Wei, Baojuan Sun, Ruifei Duan, Junxi Wang

Semiconductor Lighting Research and Development Center, Institute of Semiconductors, Chinese Academy of Sciences, Beijing 100083, China

Abstract

A method to obtain high quality semipolar $\{10\bar{1}\bar{3}\}$ GaN grown on m-plane sapphire is presented, which is similar to two-step nanoepitaxial lateral overgrowth (2S-NELOG) by combining TiN interlayer and self-assembled SiO_2 nanospheres. For the 2S-NELOG semi-GaN, the root-mean-square roughness (RMS) is 1.8 nm with the scan of 5×5 μm^2. The reduction of defect density is demonstrated by high resolution X-ray diffractometer (HRXRD) and transmission electron microscopy (TEM). The full widths at half maximum (FWHMs) of on-axis X-ray rocking curves (XRCs) are 381 and 524 arcsec, respectively, rocking toward the $[30\bar{3}\bar{2}]$ direction and the $[1\bar{2}10]$ direction, and the anisotropy of mosaic is lower compared with planar and TiN semi-GaN. In addition, Raman analyses also show partial relaxation of the stress in the 2S-NELOG semi-GaN.

---

[*] Corresponding author: **tbwei@semi.ac.cn** (T. B. Wei)

Tel: +86-10-82305247, Fax: +86-10-82305304

1. Introduction

Semipolar GaN layers have attracted considerable attention as means of reducing the quantum-confined Stark effect in GaN-based light emitting diodes (LEDs) **[1-2]**. Recently, semipolar blue LEDs have been demonstrated to approach their c-plane counterparts **[3]**. Especially, the output power and external quantum efficiency are the highest ever reported for green LEDs grown on semipolar GaN **[4].** However, these devices are usually grown on bulk GaN substrates, which are obtained by slicing thick c-GaN grown by hydride vapor phase epitaxy (HVPE). Considering the limited availability of bulk GaN substrates due to their high cost and small size, heretoepitaxy is still an attractive approach to obtain semipolar GaN. Unfortunately, heteroepitaxial semipolar GaN films typically contain very high defect density, such as basal plane stacking faults (BSFs) in the range of 10^5 cm^{-1}, partial dislocations (PDs) in the range of 10^{10} cm^{-2} **[5]**, which is believed to limit the room internal quantum efficiency of semipolar InGaN/GaN structures **[6]**. Although semipolar $\{10\bar{1}\bar{3}\}$ GaN films have been grown on spinel substrate and m-plane sapphire **[7-8]**, the crystal quality of as-grown films must be further improved for device growth.

Epitaxial lateral overgrowth (ELOG) is a widely used technique to obtain high quality polar GaN, which has also been applied to grow low defect density of nonpolar and semipolar GaN **[9-11]**. Nevertheless, conventional ELOG process requires ex situ photolithographic steps, which increases the process complexity and cost that mass production is difficult. Alternative method is interlayer technique, such as CrN, ScN, TiN interlayer in heteroepitaxial semipolar GaN films **[12-14]**. This is similar to ELOG process, and the interlayer is used as the mask due to their porous network structure. Recently, self-assembled nanosphere technique also exhibits an improvement of polar or nonpolar GaN epilayer quality due to nanoepitaxial lateral overgrowth (NELOG) **[15-17]**. In addition, it is reported that two-step ELOG can further reduce the density of defects in GaN growth **[18-19]**. However, this requires more troublesome processes. In this paper, a method to obtain high quality semipolar $\{10\bar{1}\bar{3}\}$ GaN grown on m-plane sapphire is presented, which is similar to two-step nanoepitaxial lateral overgrowth (2S-NELOG) by combining TiN interlayer and self-assembled SiO_2 nanospheres. It is worthy of noting that interlayer and self-assembled nanosphere techniques similar to NELOG are nonlithographic nanoheteroepitaxy to obtain large size and uniform films due to nanometer-scale feature, which is cost-efficient for mass production compared with the conventional ELOG.

2. Experimental

The fabrication process and schematic diagram of the samples were shown in Fig. 1. All samples were grown by HVPE in the home-designed horizontal quartz reactor. Ammonia gas (NH_3) and GaCl which generated by reactions between hydrogen chloride (HCl) gas and liquid Ga are used as the nitrogen and gallium source, respectively. Nitride gas (N_2) is used as carried gas in all experiments. First of all, nitridation treatment was carried out at 1080 ℃ for 8 min in a NH_3 environment prior to epitaxial growth. Then, the temperature was reduced to 930℃ and a buffer layer was grown for 5 min at a V/III ratio of 50 with HCl rate of 10 sccm. Subsequently, the temperature was raised to 1050℃, and about 5-μm GaN layer was grown at an enhanced V/III ratio with HCl rate of 40 sccm. This was used as GaN template in next growth. Secondly, a 10-nm TiN film was deposited on the GaN template by Discovery Magnetron Sputter Deposition systems, which is of wurtzite structure with porous network surface Morphology similar to previous report **[20]**. Thirdly, close-packed SiO_2 nanospheres were formed by self-assembled at the air-water interface and were transferred to the underlying TiN layer. The detailed process was described in ref. **[21]**. Then, the separate nanospheres were obtained by inductively coupled plasma (ICP) etching with CF_4 as etching gas. Diameter of nanospheres was determined by the process time of ICP etching. Finally, obtained substrate as shown in Fig. 1(d) is grown again under the same growth condition as the first growth by HVPE with the exception of nitridation step. About 50-μm GaN layer is obtained after 60 min growth and is labeled as 2S-NELOG semi-GaN. For the purpose of comparison, two samples respectively grown on a planar m-sapphire and GaN template with TiN interlayer were also prepared (labeled as planar semi-GaN and TiN IL semi-GaN, respectively), which is of the same thickness as 2S-NELOG semi-GaN. The crystallographic orientation and the crystalline quality of the as-grown GaN layers were studied by a high resolution X-ray diffractometer (HRXRD) using Cu $K_{\alpha1}$ radiation. Morphology character of the as-grown films was characterized by JSM-5600LV scanning electronic microscope (SEM) and Nanoscope III atomic force microscope (AFM). The structural character of 2S-NELOG semi-GaN was investigated by transmission electron microscopy (TEM). Cross-section TEM specimens were prepared by a focused ion beam (FIB) instrument, and the observations were carried out on FEI Tecnai G2 F20 microscope operated at 200 kV accelerating voltage. The stress of the semipolar

GaN was analyzed by Raman spectroscopy.

3. Results and discussion

Top-view SEM image of separate nanospheres is shown in Fig. 2(a). Regular nanospheres with the average diameter of 500 nm are obtained on the underlying TiN layer followed by 200 s etching time. Cross-section and surface SEM images of 2S-NELOG semi-GaN are shown in Fig. 2(b) and Fig. 2(c). Different layers can be seen from cross-section images and the surface of the sample is rather smooth. AFM images of all samples are illustrated in Fig. 2(d-f). The root-mean-square (RMS) roughness of the planar semi-GaN is 4.6 nm with the scan of $5 \times 5\ \mu m^2$. However, the RMS is reduced to 3.2 nm and 1.8 nm for TiN IL and 2S-NELOG semi-GaN, respectively. As far as the planar semi-GaN is concerned, the striated surface morphology perpendicular to the GaN $[30\bar{3}\bar{2}]$ direction is clearly visible. In contrast, the number of stripes reduces for the 2S-NELOG semi-GaN. It should be noted that the striated features are typical for nonpolar and semipolar GaN epilayers, which could prove strong morphological anisotropy and reflect density of BSFs **[22-23].** These results suggest that the crystalline quality of the GaN layer can be improved, which ascribes to using TiN interlayer and self-assembled SiO_2 nanospheres similar to 2S-NELOG.

The surface orientation is determined using 2θ-ω scans that reveal the $\{10\bar{1}\bar{3}\}$ plane for all samples. The detailed investigations have been reported in ref. **[24]**. It is reported that the dislocations in semipolar GaN epilayers include Frank-Shockley PDs with the Burgers vector b = 1/6 $<20\bar{2}3>$ (90%), Shockley PDs with b = 1/3 $<10\bar{1}0>$ (8%) and perfect dislocations of a-type with b = 1/3 $<11\bar{2}0>$ (2%) **[25-26]**. In addition, semipolar epilayers commonly contain BSFs and PSFs, which is I_1-type BSFs bounded by Frank-Shockley PDs, I_2-type BSFs bounded by Shockley PDs and prismatic stacking faults (PSFs) with the displacement vector R = $1/3<11\bar{2}0>$. The invisibility criteria of the defects under XRD or TEM has been studied, and $\mathbf{g}\cdot\mathbf{R} = n$ are used for BSFs as well as $\mathbf{g}\cdot\mathbf{b} = 0$ for PDs, where g is the reflection, R is the stacking fault displacement vector, b is the dislocation Burgers vector and n is an integer (including zero) **[27-29]**. For semipolar GaN, dislocations Burgers, stacking faults displacement vector and extinction rules under XRD or TEM are summarized in Table I. In order to characterize the defects of semipolar GaN layers, double-crystal X-ray rocking curves (XRCs) for on-axis and off-axis diffraction planes were carried out by HRXRD, where a 1.0×0.5 mm slit was employed for light source.

Figure 3(a) shows on-axis XRCs of the semipolar $\{10\bar{1}\bar{3}\}$ GaN with incident beam direction of $[30\bar{3}\bar{2}]$. It can be seen that the full width at half maximum (FWHM) reduces and that the intensity of XRD increases when TiN IL or 2S-NELOG processes are applied. Fig. 3(b) shows the FWHMs of off-axis (000n) XRCs with different order n (2, 4, 6), which has an inclination angle 32^0 with respect to $\{10\bar{1}\bar{3}\}$ plane. Compared with that of the planar and TiN IL semi-GaN, the FWHMs of (000n) XRCs for the 2S-NELOG semi-GaN markedly decreased. According to the invisibility criteria as shown Table I, the Shockley PDs and perfect dislocations of a-type are visible under on-axis XRCs with incident beam direction of $[30\bar{3}\bar{2}]$, in contrast, and all stack faults are invisible. Also, only Frank-Shockley PDs is visible under off-axis (000n) XRCs. Therefore, these results indicate that the density of dislocations in the 2S-NELOG semi-GaN is decreased effectively. Fig. 3(c) shows FWHMs of the on axis $\{10\bar{1}\bar{3}\}$ XRCs as a function of the azimuthal angle ϕ. The angle ϕ was set at 0^0 and 90^0 when the rocking direction was parallel to $[30\bar{3}\bar{2}]$ and the in-plane $[1\bar{2}10]$, respectively. All samples exhibits anisotropy of mosaic in the on-axis rocking curves, which is often observed in semipolar GaN films caused by the growth rate in different orientation **[7]**. For the 2S-NELOG semi-GaN, the FWHMs of on- axis XRCs are 381 and 524 arcsec respectively rocking toward the $[30\bar{3}\bar{2}]$ direction and the $[1\bar{2}10]$ direction, which is the lowest in all samples. Meanwhile, the anisotropy of mosaic is of the same trend, which is ascribed to the reduction of the dislocations.

To evaluate the BSFs in the semipolar $\{10\bar{1}\bar{3}\}$ GaN, XRCs of off-axis $(n0\bar{n}0)$ planes, which has an inclination angle 58^0 with respect to $\{10\bar{1}\bar{3}\}$ plane, were carried out. Fig. 3(d) shows the FWHMs of $(n0\bar{n}0)$ XRCs with different order n increased from 1 to 3. Compared with that of the planar and TiN IL semi-GaN, the FWHMs of $(n0\bar{n}0)$ XRCs for the 2S-NELOG semi-GaN markedly decreased. It should be noted that I_1 and I_2 BSFs should affect the $(10\bar{1}0)$ and $(20\bar{2}0)$ reflections, whereas neither should affect the $(30\bar{3}0)$ reflection. Thus, these results indicate that the density of BSFs has been reduced in 2S-NELOG semi-GaN. The previous reports have demonstrated that TiN IL or SiO_2 nanospheres as the mask can reduce the defect density in heteroepitaxial semipolar GaN, which is similar to nanolateral epitaxial overgrowth **[14, 16]**. So it is reasonalbe to speculate that the reduction of defect density in 2S-NELOG semi-GaN is due to two-step nanolateral epitaxial overgrowth, where TiN IL is used as the one mask and SiO_2 nanospheres as the other mask as shown in Fig. 1(e).

Cross-section TEM images of 2S–NELOG semi-GaN taken near the $[11\bar{2}0]_{GaN}$ zone axis are performed to further investigate the structure character and growth mechanism. At first, selected area diffraction (SAD) patterns were taken and shown in Fig. 4(a), which is used to determine (0002) and $(01\bar{1}0)$ plane. Figure 4(b) presents a multiple beam bright-field (BF) image, which reveals the structure of the sample. Along the growth orientation, different layers are obviously seen, including GaN-1 at the bottom, the TiN interlayer (a magnified view of region Ⅰ as shown in the inset), SiO_2 nanospheres and GaN-2. Figure 4(c) shows dark-field (DF) image with diffraction vector g = (0002). As far as diffraction vector in the c-plane is concerned, BSFs, Shockley PDs and perfect dislocation of a-type are invisible, while Frank-Shockley PDs are visible. One can see that the density of Frank-Shockley PDs reduces markedly for GaN-2 layer, which is attributed to the block of TiN interlayer and SiO_2 nanospheres and accords with the results of XRD. Figure 4(d) shows DF image at a magnified view of region Ⅱ with diffraction vector g = $(1\bar{1}00)$. It should be noted that BSFs is visible, in contrast, and PSFs is invisible in this case. Only a part of BSFs reoccurs at the surface of SiO_2 nanospheres in GaN-2 layer. Because all TEM images are taken round the interface, we speculate the density of defects should further be reduced with the increase of film thickness.

The stress of the semipolar GaN is analyzed by Raman spectroscopy. Figure 5(a) shows the results of Raman scattering analysis for all samples. The E_2-high phonon modes of are located at 567.3 cm^{-1} for 2S-NELOG semi-GaN, which is the lowest in three samples. The E_2-high peak value of the unstrained GaN is believed to be 567.0 $\pm$ 0.1 cm^{-1} **[30].** The result indicates the partial relaxation of the stress in 2S-NELOG semi-GaN. Figure 5(b) and 5(c) show cross-sectional SEM images of TiN IL semi-GaN and 2S-NELOG semi-GaN, respectively. Some holes occur at the interface for TiN IL semi-GaN, and SiO_2 nanospheres deform after regrowth for 2S-NELOG semi-GaN, so it is reasonable to speculate that the stress is partially relaxed due to the holes or deformation.

4. Conclusion

In conclusion, as far as 2S-NELOG semi-GaN is concerned, not only the defect density reduces, but the stress is partially relaxed compared with the planar and TiN IL seimi-GaN. Furthermore, the anisotropy of mosaic in the semipolar GaN is also obviously improved by 2S-NELOG growth. Interestingly, this method is a nonlithographic process, and 2S-NELOG can be realized only by once re-growth. It suggests this method is a useful and valuable technique to obtain high quality semipolar GaN.

Acknowledgments

This work was supported by the National Natural Sciences Foundation of China under Grants 61274040 and 51102226, by the National Basic Research Program of China under Grant 2011CB301904 and by the National High Technology Program of China under Grants 2014AA032605.

References

[1] A. Chakraborty, T. J. Baker, B. A. Haskell, F. Wu, J. S. Speck, S. P. Denbaars, S. Nakamura, U. K. Mishra, Jpn. J. Appl. Phys. 44 (2005) L945

[2] N. Okada, K. Uchida, S. Miyoshi, K. Tadatomo, Phys. Status Solidi A 209, (2012) 469

[3] Y. Zhao, J. Sonoda, C. C. Pan, S. Brinkley, I. Koslow, K. Fufito, H. Ohta, S. P. DenBaars, S. Nakamura, Appl. Phys. Express 3 (2010) 102101

[4] S. Yamamoto, Y. Zhao, C. C. Pan, R. B. Chung, K. Fujito, J. Sonoda, S. P. DenBaars, S. Nakamura, Appl. Phys. Express 3 (2010) 122102

[5] T. J. Baker, B. A. Haskell, F. Wu, J. S. Speck, S. Nakamura, Jpn. J. Appl. Phys. 45 (2006) L154

[6] N. P. Hylton, P. Dawson, C. F. Johnston, M. J. Kappers, J. L. Hollander, C. McAleese, C. J. Humphreys, Phys. Status Solidi C S2 (2009) S727

[7] T. J. Baker, B. A. Haskell, F. Wu, P. T. Fini, J. S. Speck, S. Nakamura, Jpn. J. Appl. Phys. 44 (2005) L920

[8] T. B. Wei, Q. Hu, R. F. Duan, X. C. Wei, Z. Q. Huo, J. X. Wang, Y. P. Zeng, G. H. Wang, J.M. Li, J. Cryst Growth 311 (2009) 4153

[9] B. A. Haskell, F. Wu, M. D. Craven, S. Matsuda, P. T. Fini, T. Fujii, K. Fujito, S. P. DenBaars, J. S. Speck, S. Nakamura, Appl. Phys. Lett. 83 (2003) 644

[10] B. A. Haskell, T. J. Baker, M. B. McLaurin, F. Wu, P. T. Fini, S. P. DenBaars, J. S. Speck, S. Nakamura, Appl. Phys. Lett. 86 (2005) 111917

[11] P. De. Mierry, N. Kriouche, M. Nemoz, G. Nataf, Appl. Phys. Lett. 94 (2009) 191903

[12] K. W. Liu, S. J. Chang, S. J. Young, T. H. Hsueh, H. Hung, Y. C. Mai, S. M. Wang, Y. Z. Chen,

J. Electrochen. Soc. 158 (2011) H983

[13] C. F. Johnston, M. A. Moram, M. J. Kappers, C. J. Humphreys, Appl. Phys. Lett.94 (2009) 161109

[14] S. R. Xu, Y. Hao, L. A. Yang, J. C. Zhang, J. S. Xue, X. Y. Xue, Z. Y. Liu, Z. Y. Lin, J. C. Ma, P. X. Li, J. T. Li, Q. He, Jpn. J. Appl. Phys. 50 (2011) 115502

[15] S. J. An, Y. J. Hong, G. C. Yi, Y. J. Kim, D. K. Lee, Adv. Mater.18 (2006) 2833

[16] Q. M. Li, J. J. Figiel, G. T. Wang, Appl. Phys. Lett. (2009) 231105

[17] S. W. Pak, D. U. Lee, E. K. Kim, S. H. Park, K. Joo, E. Yoon, J. Cryst Growth 370 (2013) 78

[18] P. Vennéguès, B. Beaumont, V. Bousquet, M. Vaille, P. Gibart, J. Appl. Phys. 87 (2000) 4175

[19] J. L. Hollander, M. J. Kappers, C. J. Humphreys, Phys. B (2007) 401

[20] Y. Fu, F. Yun, Y. T. Moon, Ü. Özgür, J. Q. Xie, X. F. Ni, N. Biyikli, H. Morkoc, L. Zhou, D. J. Smith, C. K. Inoki, T. S. Kuan, Appl. Phys. Lett. 99 (2006) 033518

[21] V. Nicolas, G. Sebastian, L. Katharina, K.W. Clemens, Macromol. Chem. Phys. 212 (2011) 1719

[22] B. A. Haskell, F. Wu, M. D. Graven, S. Matsuda, P. T. Fini, T. Fujii, K. Fujito, S. P. DenBaars, J. S. Speck, S. Nakamura, Appl. Phys. Lett. 83 (2003) 644

[23] T. B. Wei, R. F. Duan, J. X. Wang, J. M. Li, Z. Q. Huo, J. K. Yang, Y. P. Zeng, Jpn. J. Appl. Phys. 47 (2008) 3346

[24] T. B. Wei, Q. Hu, R. F. Duan, X. C. Wei, J. K. Yang, J. X. Wang, Y. P. Zeng, G. H. Wang, J. M. Li, J. Electrochem. Soc. 157 (2010) H721

[25] Y. A. R. Dasilva, M. P. Chauvat, P. Ruterana, L. Lahourcade, E. Monroy, G. Nataf, J. Phys.: Condens. Matter 22 (2010) 355802

[26] T. Zhu, C. F. Johnston, M. J. Kappers, R. A. Oliver, J. Appl. Phys. 108 (2010) 083521

[27] M. A. Moram, C. F. Johnston, J. L. Hollander, M. J. Kappers, J. Humphreys, J. Appl. Phys. 105 (2009) 113501

[28] Q. Sun, B. Leung, C. D. Yerino, Y. Zhang, J. Han, Appl. Phys. Lett. 95 (2009) 231094

[29] P. Vennegues, Z. Bougrioua, T. Guehen, Jpn. J. Appl. Phys. 46 (2007) 4089

[30] A. R. Goni, H. Siegle, K. Syassen, C. Thomsen, J. M. Wagner, Phys. Rev. B 64 (2001) 035205

Figure Captions

Figure 1 A schematic graph of the fabrication process: (a) GaN templates grown on m-plane sapphire by HVPE. (b) TiN film by magnetron sputtering deposition. (c) close-packed nanospheres by self-assembled. (d) The separate nanospheres on the underlying TiN layer. **(e)** A schematic diagram of 2S-NELOG.

Figure 2 (a) Top-view SEM image of nanospheres suffered from 200 s ICP etching. (b) Cross-section and (c) surface SEM images of 2S-NELOG semi-GaN. AFM ($5\times5\ \mu m^2$) images of (d) planar semi-GaN, (e) TiN semi-GaN and (f) 2S-NELOG semi-GaN.

Figure 3 (a) On-axis XRCs of $\{10\bar{1}\bar{3}\}$ GaN with incident beam direction of $[30\bar{3}\bar{2}]$. (b) FWHMs of (000n) XRCs (n=2, 4, 6). (c) FWHMs of the on-axis XRCs of $\{10\bar{1}\bar{3}\}$ GaN as a function of the azimuth angle, ϕ. (d) FWHMs of $(n0\bar{n}0)$ XRCs (n=1, 2, 3).

Figure 4 Cross-section TEM images of 2S-NELOG semi-GaN taken near the $[11\bar{2}0]_{GaN}$ zone axis. (a) Selected area diffraction (SAD) patterns. (b) Multiple beam BF image, the inset shows a magnified view of Region **I**. (c) DF image at (b) region, g = (0002). (d) DF image at a magnified view of region Ⅱ, g = $(1\bar{1}00)$.

Figure 5 (a) Raman scattering analyses of semipolar $\{10\bar{1}\bar{3}\}$ GaN. The inset shows a magnified view of red region. Cross-sectional SEM images of (b) TiN IL semi-GaN and (c) 2S-NELOG semi-GaN

Table 1 Dislocations Burgers, stacking faults displacement vector and extinction rules under XRD or TEM

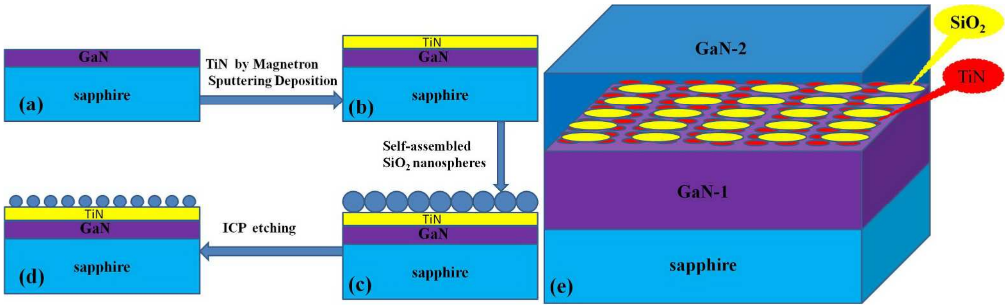

A schematic graph of the fabrication process: (a) GaN templates grown on m-plane sapphire by HVPE. (b) TiN film by magnetron sputtering deposition. (c) close-packed nanospheres by self-assembled. (d) The separate nanospheres on the underlying TiN layer. (e) A schematic diagram of 2S-NELOG.
962x289mm (72 x 72 DPI)

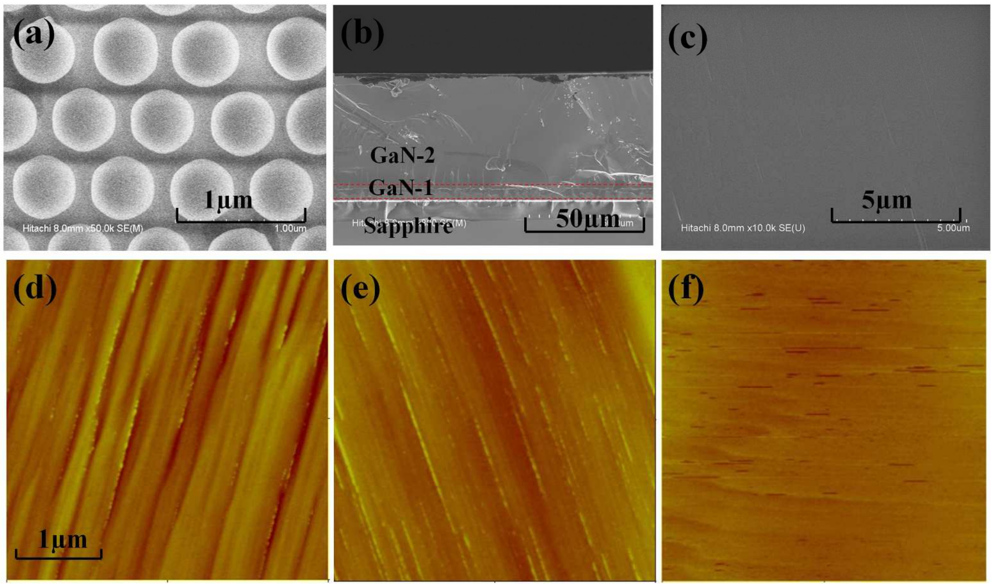

(a) Top-view SEM image of nanospheres suffered from 200 s ICP etching. (b) Cross-section and (c) surface SEM images of 2S-NELOG semi-GaN. AFM (5×5 µm2) images of (d) planar semi-GaN, (e) TiN semi-GaN and (f) 2S-NELOG semi-GaN.
878x516mm (72 x 72 DPI)

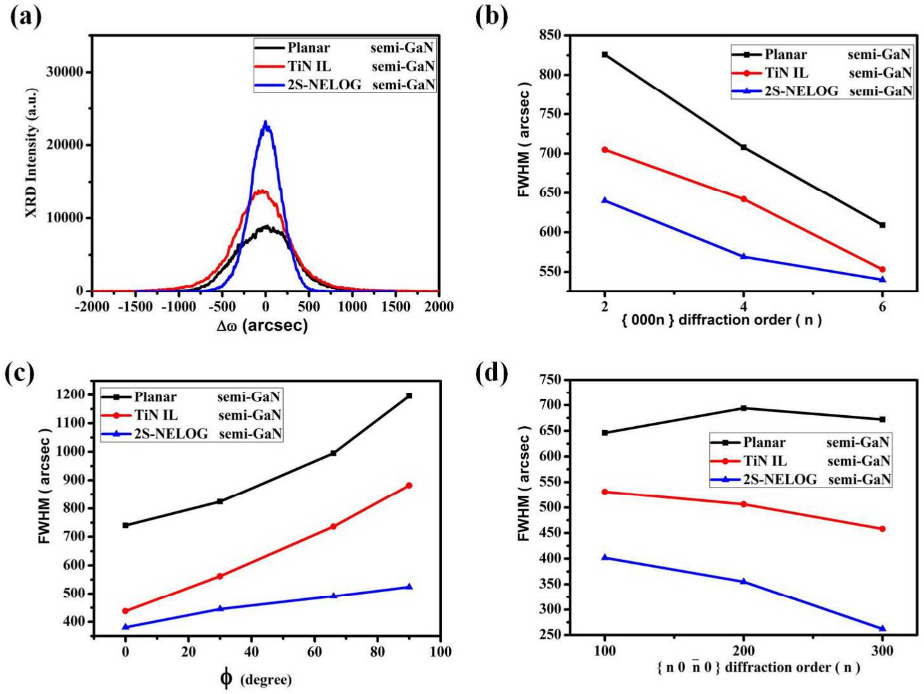

(a) On-axis XRCs of {10(1)¯3¯} GaN with incident beam direction of [303¯2¯]. (b) FWHMs of (000n) XRCs (n=2, 4, 6). (c) FWHMs of the on-axis XRCs of {10(1)¯3¯} GaN as a function of the azimuth angle, Φ (d) FWHMs of (n0n¯0) XRCs (n=1, 2, 3).
735x520mm (72 x 72 DPI)

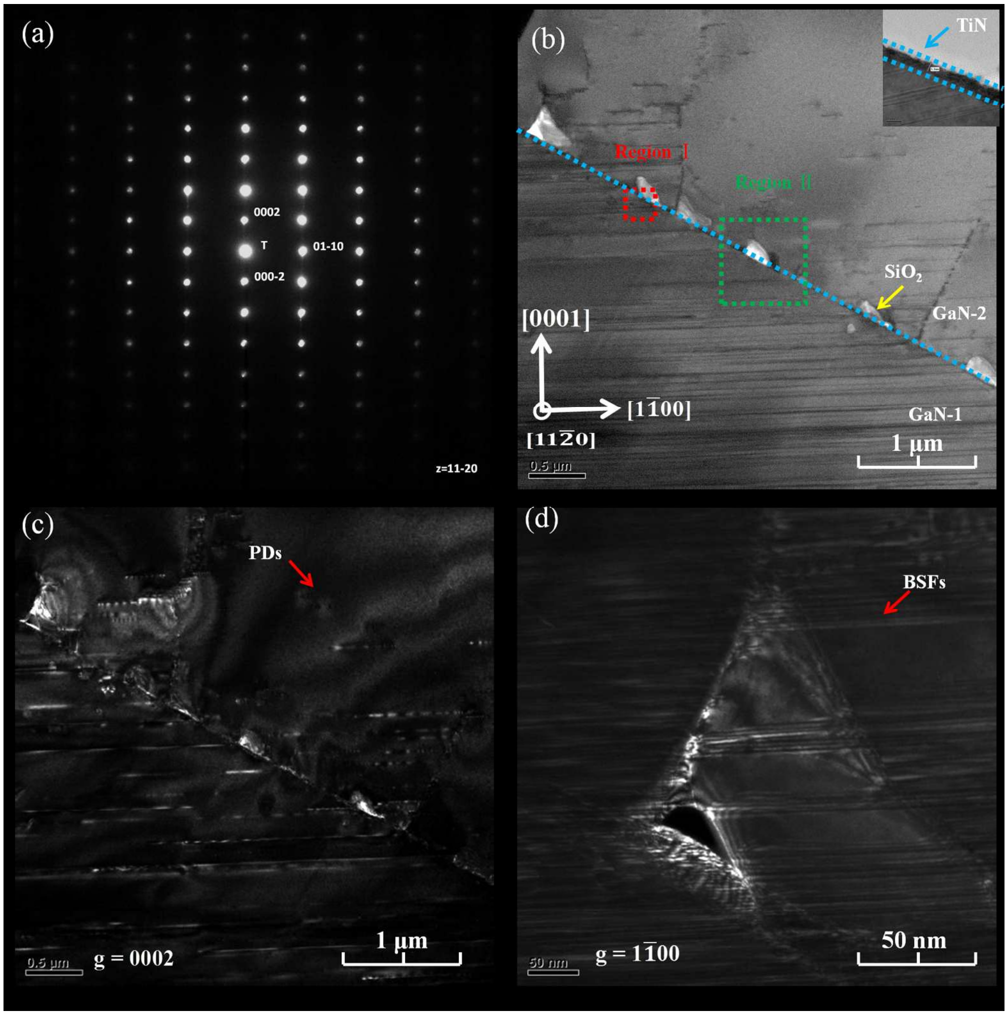

Cross-section TEM images of 2S-NELOG semi-GaN taken near the [112¯0]GaN zone axis. (a) Selected area diffraction (SAD) patterns. (b) Multiple beam BF image, the inset shows a magnified view of Region I. (c) DF image at (b) region, g = (0002). (d) DF image at a magnified view of regionⅡ, g = (11¯00).
334x335mm (150 x 150 DPI)

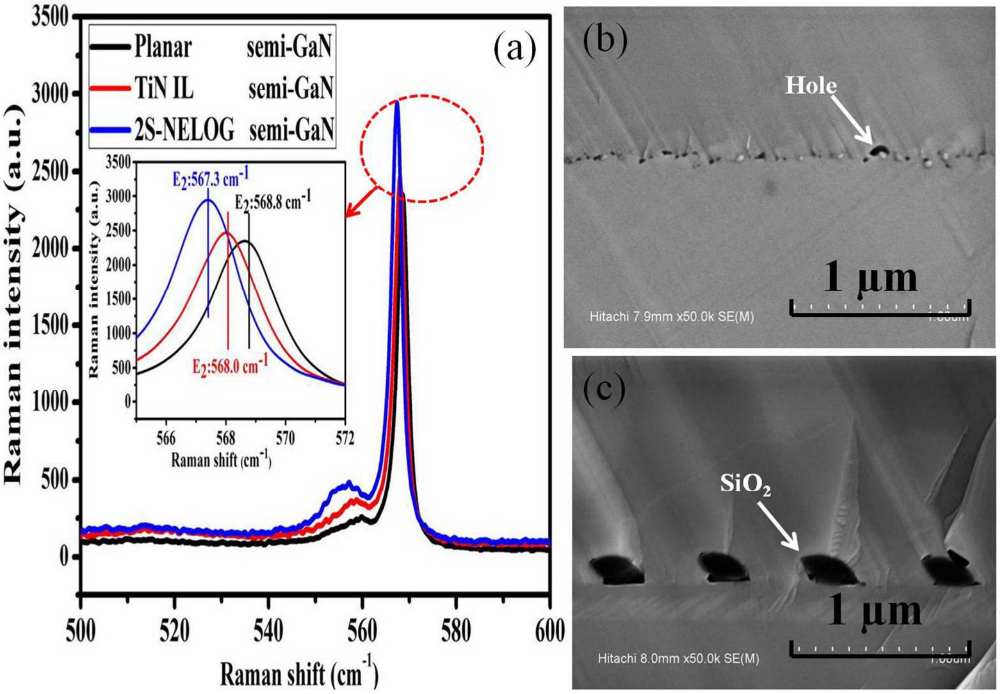

(a) Raman scattering analyses of semipolar {10(1)⁻3⁻} GaN. The inset shows a magnified view of red region. Cross-sectional SEM images of (b) TiN IL semi-GaN and (c) 2S-NELOG semi-GaN
512x359mm (72 x 72 DPI)

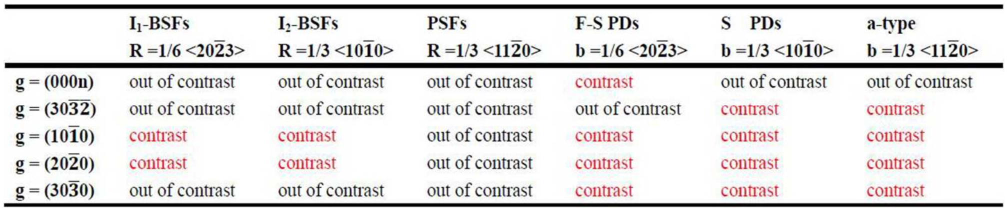

	I_1-BSFs R =1/6 <$20\bar{2}3$>	I_2-BSFs R =1/3 <$10\bar{1}0$>	PSFs R =1/3 <$11\bar{2}0$>	F-S PDs b =1/6 <$20\bar{2}3$>	S PDs b =1/3 <$10\bar{1}0$>	a-type b =1/3 <$11\bar{2}0$>
g = (000n)	out of contrast	out of contrast	out of contrast	contrast	out of contrast	out of contrast
g = ($30\bar{3}\bar{2}$)	out of contrast	out of contrast	out of contrast	out of contrast	contrast	contrast
g = ($10\bar{1}0$)	contrast	contrast	out of contrast	contrast	contrast	contrast
g = ($20\bar{2}0$)	contrast	contrast	out of contrast	contrast	contrast	contrast
g = ($30\bar{3}0$)	out of contrast	out of contrast	out of contrast	contrast	contrast	contrast

Dislocations Burgers, stacking faults displacement vector and extinction rules under XRD or TEM
412x84mm (72 x 72 DPI)